Electrical, thermal and electrochemical properties of SmBa1−xSrxCo2O5+δ cathode materials for…

Article *in* Electrochimica Acta · June 2016

DOI: 10.1016/j.electacta.2016.04.069

CITATIONS
4

READS
33

5 authors, including:

Adi Subardi
National Dong Hwa University
8 PUBLICATIONS **19** CITATIONS
SEE PROFILE

Yen-Pei Fu
National Dong Hwa University
139 PUBLICATIONS **1,673** CITATIONS
SEE PROFILE

Electrochimica Acta 204 (2016) 118–127

Contents lists available at ScienceDirect

Electrochimica Acta

journal homepage: www.elsevier.com/locate/electacta

Electrical, thermal and electrochemical properties of $SmBa_{1-x}Sr_xCo_2O_{5+\delta}$ cathode materials for intermediate-temperature solid oxide fuel cells

Adi Subardi[a,b], Ching-Cheng Chen[a], Meng-Hsien Cheng[a], Wen-Ku Chang[a], Yen-Pei Fu[a,c,*]

[a] Department of Materials Science & Engineering, National Dong Hwa University, Shou-Feng, Hualien 97401, Taiwan
[b] Department of Mechanical Engineering, STTNAS, Yogyakarta 55281, Indonesia
[c] Nanotechnology Research Center, National Dong Hwa University, Shou-Feng, Hualien 97401, Taiwan

ARTICLE INFO

Article history:
Received 27 January 2016
Received in revised form 11 April 2016
Accepted 13 April 2016
Available online xxx

Keywords:
Layered perovskite
Oxygen content
Electrical conductivity
Power density
IT-SOFCs

ABSTRACT

The effects of Sr doping on the Ba-site of $SmBaCo_2O_{5+\delta}$ in term of structure characteristics, thermal expansion coefficients (TECs), electrical properties and electrochemical performance have been investigated as cathode material for intermediate-temperature solid oxide fuel cells (IT-SOFCs). The TECs of SBSC-based cathodes are calculated from $19.8 - 20.5 \times 10^{-6}\,K^{-1}$ in the temperature range of 100–800 °C, and the TEC values decrease with increasing Sr content. The oxygen content and the average oxidation state of cobalt increase with increasing Sr content determined by the X-ray photoelectron spectroscopy (XPS) and Thermogravimetry analysis (TGA) results. At a given temperature, the electrical conductivity values are in the order as follows: SBSC55 > SBSC73 > SBSC91. This behavior might be due to the increase in electronic hole. The electrical conductivities of SBSC55 at 600 °C are distributed in the range of 660 S/cm of $p(O_2) = 0.01$ atm to 1168 S/cm of $p(O_2) = 0.21$ atm, indicating that the cathode can endure reducing atmosphere. SBSC55 with high electrical conductivity in $p(O_2) = 0.01$ atm is ascribed to SBSC55 with stable double-perovskite structure at such low oxygen partial pressure. The SBSC55 cathode showed the highest power density of 304 mW/cm^2 at operating temperature of 700 °C. Based on the electrochemical properties, SBSC55 is a potential cathode for IT-SOFCs.

1. Introduction

Solid oxide fuel cells (SOFCs) have the potential to be one of the cleanest and most efficient energy technologies for direct conversion of chemical fuels to electricity with high efficiency, low pollution emission and extensive fuel flexibility [1–3]. Traditional SOFCs operating at temperature above 900 °C limits their applications such as using expensive materials to endure high temperature [4]. Recently, most of the research work has been devoted to lowering the operating temperature around 500–600 °C; however, a lower operating temperature causes slow oxygen reduction kinetic and high over-potential at the cathode, and leads the decrease in the electrode catalytic activity for oxygen reduction reaction [5–7]. Hence, the development of new electrodes with high-electrocatalytic activity for the oxygen reduction reaction (ORR) is critical for IT-SOFCs [8,9]. Using mixed ion and electron conductors (MIECs) decreases the cathodic polarization resistance by extending the active zone of ORR from the three phase boundary (TPB) to part of the cathode-gas interface [10,11]. The ORR sites of MIECs proceed not only on the TPB between the cathode, electrolyte and gas phase but also on the two phase boundary between the cathode and gas phase [12].

Recently, it is well known that MIECs with layered perovskite such as $NdBa_{1-x}Sr_xCo_2O_{5+\delta}$ [13], $GdBa_{0.5}Sr_{0.5}Co_{2-x}Fe_xO_{5+\delta}$ [14], $PrBa_{0.5}Sr_{0.5}Co_{2-x}Fe_xO_{5+\delta}$ [15], $YBa_{0.6}Sr_{0.4}Co_2O_{5+\delta}$ [16], $SmBa_{0.5}Sr_{0.5-}Co_{1.5}Cu_{0.5}O_{5+\delta}$ have been reported as candidate materials for IT-SOFC cathodes [6]. $LnBaCo_2O_{5+\delta}$ (Ln = Y, Pr, Gd, Nd, Sm) reveal a cation-ordered double perovskite structure with stacking layers of Ln-O and Ba-O [17], and the oxygen vacancies mostly distributed in the LnO_δ layers can significantly improve the diffusivity of oxide ions in the bulk of the material, and these vacancies provide possible surface defect sites to react with molecular oxygen [18]. The above-mentioned properties can enhance the electrochemical performance of the cathode.

* Corresponding author at: Department of Materials Science & Engineering, National Dong Hwa University, Shou-Feng, Hualien 97401, Taiwan. Tel.: +886 3 863 4209; fax: +886 3 863 4200.
E-mail address: ypfu@mail.ndhu.edu.tw (Y.-P. Fu).

http://dx.doi.org/10.1016/j.electacta.2016.04.069
0013-4686/

It was reported that the substitution of Sr for Ba in $LnBaCo_2O_{5+\delta}$ layered perovskite can enhance electrical conductivity and further improve electrochemical properties of cathode. The substitution of Sr for Ba in $GdBaCo_2O_{5+\delta}$ improved chemical stability between the cathode and electrolyte, and the fast oxygen transport [19]. Mckinlay et al. found that the substitution of Sr for Ba in $YBaCo_2O_{5+\delta}$ leads a structure transform from orthorhombic to tetragonal and enhancement of electrical conductivity [20]. Meng et al. also found that Sr doping in $YBaCo_2O_{5+\delta}$ improved the electrical conductivity due to the greater amount of electronic holes originated from the increased interstitial oxygen [21].

In present study, we investigated the effects of Sr partially substituting for Ba in $SmBaCo_2O_{5+\delta}$ in the aspects of structure characteristics, thermal expansion curves, thermodynamic redox behavior, electrical properties, and electrochemical performance of $SmBa_{1-x}Sr_xCo_2O_{5+\delta}$ with respect to their applications as an IT-SOFC cathode.

2. Experimental

Material preparation for electrolyte and cathode has been reported in our group's previous published papers elsewhere [22,23]. The $Ce_{0.8}Sm_{0.2}O_{1.9}$ (SDC) electrolyte powder was synthesized by co-precipitation using $Ce(NO_3)_3{\cdot}6H_2O$ (99%, Uranus Chemical, Ltd.) and $Sm(NO_3)_3{\cdot}6H_2O$ (99%, Wako Pure Chemical Industries, Ltd.) as the starting materials. The detailed procedure regarding the preparation of SDC can refer to reference 22. $SmBa_{1-x}Sr_xCo_2O_{5+\delta}$ (x = 0.1, 0.3, 0.5) cathode powders were prepared via a solid-state reaction. To identify the samples, the abbreviations were used as SBSC91, SBSC73 and SBSC55 stood for $SmBa_{0.9}Sr_{0.1}Co_2O_{5+\delta}$, $SmBa_{0.7}Sr_{0.3}Co_2O_{5+\delta}$ and $SmBa_{0.5}Sr_{0.5}Co_2O_{5+\delta}$, respectively. Stoichiometric amounts of Sm_2O_3 (99%, Wako Pure Chemical Industries, Ltd.), $BaCO_3$ (98.8%, Showa Chemical Industries, Ltd.), $SrCO_3$ (98%, Shimakyu chemical Co., Ltd), and CoO (99.9%, Choneye Pure Chemical Co., Ltd.), powders were used as starting materials. These raw powders were mixed under ethanol and milled for 12 h using zirconia balls. The ball-milled mixture was dried and ground into a powder with mortar and pestle, and then calcined in air at 1100 °C for 4 h with a ramp rate of 3 °C/min [23]. SBSC-based cathodes were sintered in air at 1200 °C with a programmed heating rate of 5 °C/min. The sintered samples were made up over 95% of the theoretical density in all the specimens for electrical conductivity measuring with different oxygen atmosphere.

The structure of calcined $SmBa_{1-x}Sr_xCo_2O_{5+\delta}$ (x = 0.1, 0.3, 0.5) cathodes were characterized by X-ray powder diffractometer (XRD; Rigaku D/MAX–2500 V), with a scanning rate of 4°/min and scanning range of 20-80°, using a Cu Kα (1.5418 Å) radiation source. The powder pattern and lattice parameter were analyzed by Rietveld refinement using the GSAS program. The microstructures of $SmBa_{1-x}Sr_xCo_2O_{5+\delta}$ (x = 0.1, 0.3, 0.5) cathode powders and cross-section image of half-cell were observed by a field emission scanning electron microscope (SEM; Hitachi 3400N). The chemical states of the SBSC55 cathode was measured by X-ray photoelectron spectroscopy (XPS, Thermal K-alpha) using micro focus mono-chromated Al Kα X-ray as the exciting source. All the binding energies were referenced to the C 1s peak at 284.3 eV. XPS measurements were carried out in a high vacuum chamber with a pressure of 3×10^{-9} mbar.

Thermogravimetric properties of $SmBa_{1-x}Sr_xCo_2O_{5+\delta}$ (x = 0.1, 0.3, 0.5) cathode were performed by a thermogravimetric analyzer (TGA, SII TG/DTA 6300) in air with a flow rate of 100 cm^3/min. The change in oxygen content $\Delta\delta$ with varying $p(O_2)$ and temperature was calculated from the sample mass change, Δm, based on

$$\boldsymbol{\delta} = \frac{\boldsymbol{M_s \Delta m}}{\boldsymbol{M_o m}} \quad (1)$$

where M_S is the molar mass of the sample, M_O is the molar mass of oxygen, and m is the sample mass at room temperature in air [24]. The oxygen nonstoichiometry and average valence of Co were determined combined by TGA and XPS. The thermal expansion coefficients of the $SmBa_{1-x}Sr_xCo_2O_{5+\delta}$ (x = 0.1, 0.3, 0.5) specimens sintered at 1100° C were measured using a thermomechanical analyzer (TMA; Hitachi TMA7300) with a constant heating rate of 10° C/min in the temperature range of 25–800 °C in static air.

The SBSC91, SBSC73 and SBSC55 cathode paste, consisting of the cathode powder, solvent, binder, and plasticizer, were prepared by ball-mill method. A symmetrical cell of SBSC/SDC/SBSC configuration was fabricated by screen-printing technique. The SBSC-based cathode paste was applied on both sides of SDC electrolyte discs in circles of 13 mm diameter and 1 mm thick. After the cathode material was painted on the electrolyte, it was sintered at 1000 °C for 4 h in air. On one side, the cathode paste was painted as the working electrode (WE) with surface area of 0.385 cm^2. The Ag reference electrode (RE) was placed away from the WE by about 0.3-0.4 cm. The cathode counter electrode (CE) was placed on the other side of the SDC disk. The symmetrical testing cell experiments were carried out under air in temperatures ranging from 600 to 850 °C at intervals of 50 °C in a furnace. The AC impedance measurement was performed using the VoltaLab PGZ301 potentiostat with frequency applied range from 100 kHz to 0.1 Hz with 10 mV AC signal amplitude. The EIS fitting analysis was performed with the Z-view software

Button cells were measured with humidified hydrogen (3 vol% H_2O) as the fuel and air as the oxidant to evaluate the performance of the SOFCs. The current-voltage (I–V) characteristics of the single cells were collected using a digital source meter (Keithley 2420) in a temperature range of 500–800 °C at intervals of 100 °C. C. The single cells were fabricated using anode-supported fuel cell to form configuration of Ni-SDC/SDC/SBSC with a diameter of 13 mm consisted of a SDC electrolyte (15 μm), a Ni-SDC anode (1 mm) and a SBSC cathode (20 μm). The detailed procedure to fabricate a single cell can refer to our group published paper elsewhere [25].

3. Result and discussion

The XRD patterns of $SmBa_{1-x}Sr_xCo_2O_{5+\delta}$ (x = 0.1, 0.3, 0.5) cathode calcined at 1100 °C for 4 h were illustrated in Fig. 1(a). All of SBSC-based powders are identified as layered-perovskite structure without any detectable impurity phases. It indicates that partial substitution of Sr for Ba was not significantly distorted the layered perovskite structure. The Rietveld refinement data of SBSC91, SBSC73 and SBSC55 sample are shown in Fig. 1(b)-1(d), and their structure data are listed in Table 1. There are excellent agreement between the experimental data and the calculated profiles, exhibiting that cations are well ordered between Sm^{3+} and Ba^{2+}/Sr^{2+} ions in the ordered perovskite lattice [6]. The Rietveld refinement data revealed that the diffraction patterns of all samples is a tetragonal structure with space group: *P*4/*mmm*. Table 2 listed the lattice parameters of SBSC-based samples calculated by Rietveld refinement indicating that the unit cell volume decreases with increasing Sr content due to the substitution of the smaller ionic radii of Sr^{2+} for Ba^{2+} [26].

In order to describe the spectral features of the SBSC samples, the Sr 3d, O 1s, Co 2p, and Sm 3d core-level spectra are obtained, as shown in Fig. 2. All XPS spectra are fitted with a Shirley-type background subtraction method. Based on the fitting result of the O 1s peak, the oxygen ions exist in several chemical environments. There are three kinds of chemical states observed in O 1s core level spectrum in all samples. The minor peak at a low binding energy around 528.4 eV corresponds to the lattice oxygen (O_L) at normal sites of the perovskite structures [27,28], whereas the main peak around 530.7 eV corresponds to the hydroxyl and/or carbonate

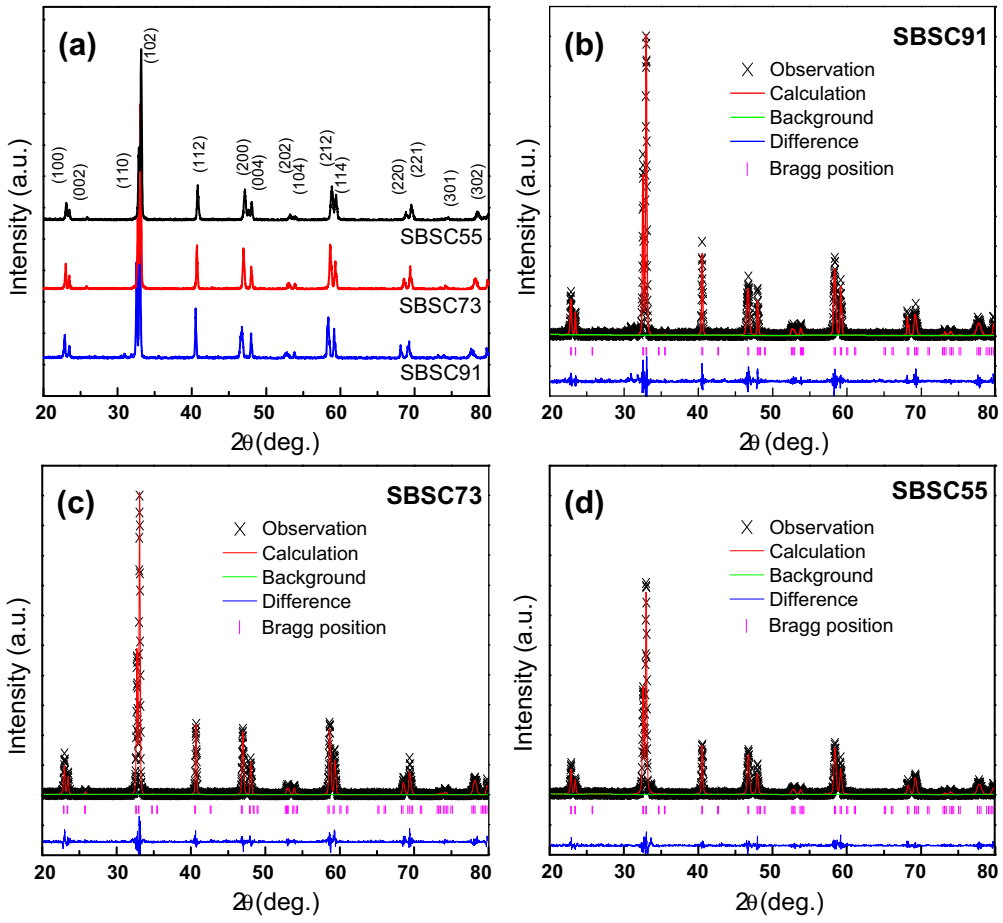

Fig. 1. (a) XRD patterns of $SmBa_{1-x}Sr_xCo_2O_{5+\delta}$ (x = 0.1, 0.3, 0.5). Observed (crosses) and calculated (solid line) XRD profiles and the difference (bottom line) between them for (b) $SmBa_{0.9}Sr_{0.1}Co_2O_{5+\delta}$ (SBSC91), (c) $SmBa_{0.7}Sr_{0.3}Co_2O_{5+\delta}$ (SBSC73), (d) $SmBa_{0.5}Sr_{0.5}Co_2O_{5+\delta}$ (SBSC55).

Table 1
Crystallographic information for SBSC-based specimens from the Rietveld refinement.

Atom	Wyckoff position	x	y	z	Uiso
SBSC91					
Sm1	1a (0 0 0)	0	0	0	0.0115
Co2	2 h ($^1/_2$ $^1/_2$ z)	0.5	0.5	0.2458	0.0020
Ba3	1b (0 0 $^1/_2$)	0	0	0.5	0.0107
O4	4i (0 $^1/_2$ z)	0	0.5	0.2219	0.0653
O5	1c ($^1/_2$ $^1/_2$ 0)	0.5	0.5	0	0.0039
O6	2 h ($^1/_2$ $^1/_2$ z)	0.5	0.5	0.4994	0.1930
Sr7	1b (0 0 $^1/_2$)	0	0	0.5	0.0439
SBSC73					
Sm1	1a (0 0 0)	0	0	0	0.0177
Co2	2 h ($^1/_2$ $^1/_2$ z)	0.5	0.5	0.2455	0.0029
Ba3	1b (0 0 $^1/_2$)	0	0	0.5	0.0123
O4	4i (0 $^1/_2$ z)	0	0.5	0.2308	0.0408
O5	1c ($^1/_2$ $^1/_2$ 0)	0.5	0.5	0	0.0081
O6	2 h ($^1/_2$ $^1/_2$ z)	0.5	0.5	0.4994	0.1930
Sr7	1b (0 0 $^1/_2$)	0	0	0.5	0.0250
SBSC55					
Sm1	1a (0 0 0)	0	0	0	0.0146
Co2	2 h ($^1/_2$ $^1/_2$ z)	0.5	0.5	0.2534	0.0007
Ba3/Sr3	1b (0 0 $^1/_2$)	0	0	0.5	0.0062
O4	4i (0 $^1/_2$ z)	0	0.5	0.2678	0.0177
O5	1c ($^1/_2$ $^1/_2$ 0)	0.5	0.5	0	0.0098
O6	2 h ($^1/_2$ $^1/_2$ z)	0.5	0.5	0.4411	0.0304

form (OH) the adsorption species [29]. Moreover, the O 1s peak about 532.8 eV is ascribed to the chemisorbed di-oxygen species (OC) [30]. The formation of OH is closely associated with the appearance of OC on the oxide surfaces due to the reaction between OC and adsorbed gaseous H_2O as a surface contaminant generated hydroxyls [31]. The detailed information regarding the binding energies of core electrons for O 1s and area % of the oxygen peaks for SBSC-based cathodes is listed in Table 3. In this study, the oxygen nonstoichiometry at room temperature was evaluate via the chemical state of Co. The Co $2p_{3/2}$ core level spectra is shown in Fig. 2(c). The spectrum can be resolved into three components such as Co^{2+} $Co^{3+}$and Co^{4+}. Based on the XPS data reported by Meng [21], the features at the binding energy of 780 eV correspond to the Co $2p_{3/2}$ signal. The average valence of Co is calculated based on the ratio of [Co^{4+}], [Co^{3+}] and [Co^{2+}] from the peak area of the singlet.

Table 2
Structure parameters of SBSC-based cathodes.

Specimens	Space group	a (Å)	b (Å)	c (Å)	V (Å^3)	R_P	R_{wp}	R_{exp}
SBSC91	*P4/mmm*	3.888	3.888	7.577	114.59	0.19	0.40	0.32
SBSC73	*P4/mmm*	3.881	3.881	7.599	114.49	0.19	0.29	0.25
SBSC55	*P4/mmm*	3.883	3.883	7.580	114.30	0.18	0.28	0.27

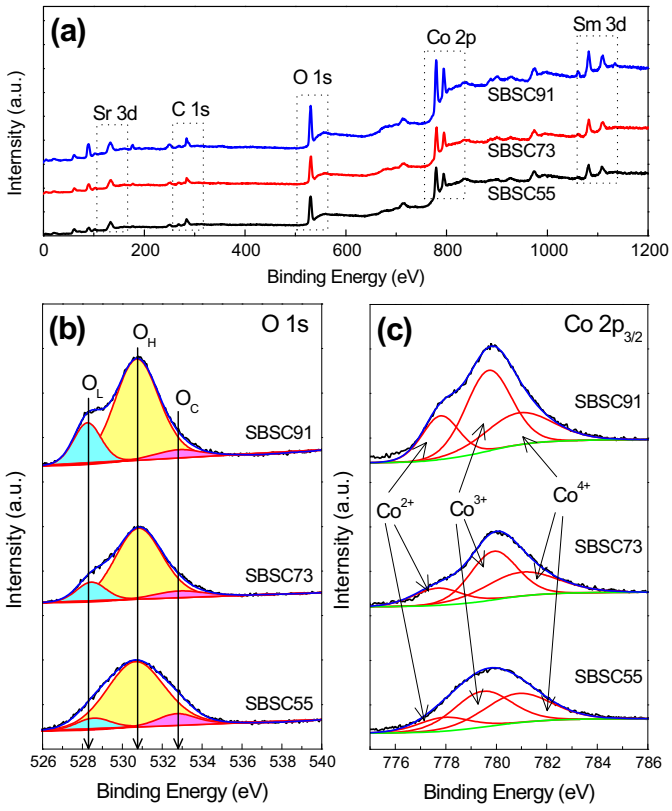

Fig. 2. XPS spectra for the SBSC-based specimens: (a) wide-survey spectrum; (b) O 1s core-level, and (c) Co 2p core-level.

The calculated average valence of Co is +3.07, +3.18 and +3.26 for SBSC91, SBSC73 and SBSC55, respectively. The 5 + δ value evaluated from XPS for SBSC91, SBSC73 and SBSC55 is about 5.57, 5.68 and 5.76, respectively. The data regarding the binding energies of Co 2p, average valence of Co and oxygen content (5 + δ) for SBSC-based cathodes are listed in Table 4.

To prove the oxygen content (5 + δ) for cathodes, thermogravimetric analysis were carried in air. The changes in mass and oxygen content (5 + δ) as a function of temperature for SBSC cathode were shown in Fig. 3. The weight loss upon heating was due to a partial loss of lattice oxygen and along with a reduction of Co^{4+} to Co^{3+} or Co^{3+} to Co^{2+} with increased temperature, so that the oxygen content, 5 + δ, decreased with temperature [32–34]. With increasing the temperature, the weight loss and the magnitude of oxygen loss were gradually increased for all samples. As shown in Fig. 3(a), the weight loss from room temperature to around 300◦C is attributed to desorption of the absorbed water for all samples. When temperature increases above the certain temperature, the magnitude of weight loss is dramatic. The certain temperature implies that the specimen start to lose lattice oxygen significantly [35]. The temperature depends on the substitution amount of Sr for Ba in $SmBa_{1-x}Sr_xCo_2O_{5+\delta}$ specimens. As increasing the substitution amount of Sr, the threshold temperatures to lose lattice oxygen is decreased. The threshold temperatures for significant oxygen loss for SBSC91, SBSC73 and SBSC55 are around 310, 280 and 260 °C, respectively. According to XPS result, the initial oxygen contents (5 + δ) for SBSC91, SBSC73 and SBSC55 are 5.57, 5.68 and 5.76, respectively at room temperature. The detailed oxygen contents as function of temperature are listed in Table 5. The initial oxygen content increases from 5.57 to 5.76 with increasing Sr content. In this study, the ionic radii of Sm^{3+}, Sr^{2+} and Ba^{2+} cations with coordination number of 6 are 0.96 Å, 1.18 Å and 1.35 Å, respectively. Obviously, the ionic-size difference between Sm^{3+} (0.96 Å) and Sr^{2+} (1.18 Å) is smaller than that between Sm^{3+} (0.96 Å) and Ba^{2+} (1.35 Å), leading the consequent perturbation of the ordering between the Sm^{3+} and Ba^{2+} layers. The high oxygen content

Table 3
The binding energies of core electrons for O 1s and area % of the oxygen peaks for SBSC-based cathodes from XPS.

Compositions	Binding energy distribution					
	O_L		O_H		O_C	
	Binding energy (eV)	Percentage of total O (%)	Binding energy (eV)	Percentage of total O (%)	Binding energy (eV)	Percentage of total O (%)
SBSC91	528.26	20.02	530.72	76.18	532.91	3.80
SBSC73	528.46	14.43	530.83	80.34	532.92	5.23
SBSC55	528.59	9.04	530.67	83.08	532.75	7.88

Table 4
The binding energies of the core electrons for Co $2p_{3/2}$, area % of Co peaks, average valence of Co and oxygen content for SBSC-based cathodes from XPS.

Specimens	Co $2p_{3/2}$	Binding energy (eV)	Percentage of total Co (%)	Average valence of Co	Oxygen Content (5 + δ)
SBSC91	Co^{4+}	780.88	28.9	3.07	5.57
	Co^{3+}	779.68	49.5		
	Co^{2+}	777.78	21.6		
SBSC73	Co^{4+}	780.97	35.7	3.18	5.68
	Co^{3+}	779.88	47		
	Co^{2+}	777.66	17.3		
SBSC55	Co^{4+}	780.83	41.4	3.26	5.76
	Co^{3+}	779.44	43.5		
	Co^{2+}	777.92	15.1		

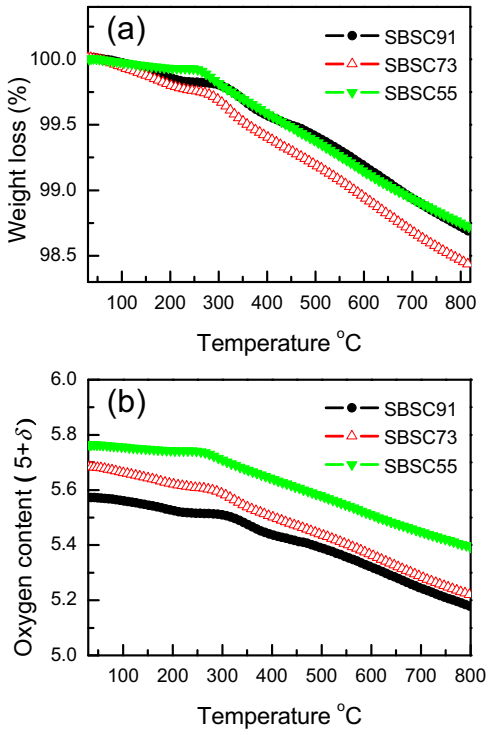

Fig. 3. (a) Thermogravimetric data and (b) oxygen content (5-δ) for SBSC-based cathodes as a function of temperature in air.

Table 5
The oxygen content (5 + δ) of SBSC-based cathodes as a function of temperature in air.

Specimens	Oxygen content (5 + δ)			
	Temperature (°C)			
	200 °C	400 °C	600 °C	800 °C
SBSC91	5.53	5.44	5.32	5.18
SBSC73	5.62	5.50	5.36	5.22
SBSC55	5.74	5.64	5.51	5.39

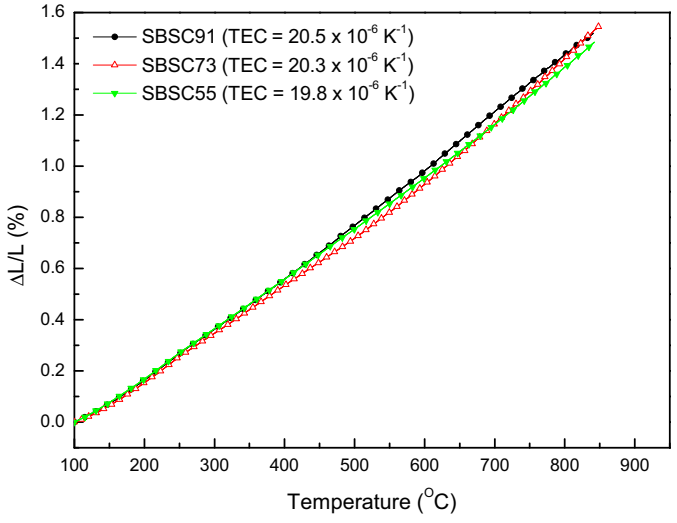

Fig. 4. Thermal expansion curves of SBSC-based cathodes as a function of temperature from 100 to 800 °C in air.

Table 6
TEC values of the SBSC-based cathodes.

Specimens	TEC × 10^{-6} (K^{-1})		
	100–800 °C	100–300 °C	300–800 °C
SBSC91	20.5	18.1	21.5
SBSC73	20.3	18.2	21.0
SBSC55	19.8	18.5	20.4

possibly cause the high diffusivity of oxide ions in the bulk and the enhanced surface activity of ORR [36].

Thermal expansion coefficient (TEC) is an important property for cathode material, as it governs the performance of a single cell. A bulk thermal expansion curves for SBSC91, SBSC73 and SBSC55 were conducted from room temperature to 800◦C using a thermomechanical analyzer, as shown in Fig. 4. The SBSC-based specimens show a linear expansion in the low temperature region (100–300 °C) and a slight increase in slope at higher temperatures region (300–800 °C). At higher temperature, a part of the smaller Co^{4+} were reduced to larger Co^{3+} or Co^{2+} with a loss of oxygen, Co^{3+} ions are easy to transit from low-spin to high-spin state [37,38]. The average TEC values of the SBSC-based specimens are listed in Table 6. The TEC values were calculated for three different temperature regions: 100-800, 100–300 and 300–800 °C. The TEC values calculated from 100 to 800 °C for SBSC91, SBSC73 and SBSC55 were 20.5 × 10^{-6}, 20. 3 × 10^{-6} and 19.8 × 10^{-6} K^{-1}, respectively. In the low-temperature region, 100–300 °C, TEC values decrease with increasing Sr content, which could be due to the replacement of the ionic Ba–O bonds with the ionic Sr–O bonds. However, in the high–temperature region, 300–800 °C, where oxygen loss occurs, TEC values increase with increasing Sr content, which can be related to the spin-state transition associated with the Co^{3+} ions [39]. Generally speaking, substituting Sr^{2+} for Ba^{2+} resulted in a lower thermal expansion coefficient. As increasing Sr^{2+} substitution amount for Ba^{2+}, the TEC values were decreased. Generally, cobalt-based perovskites with a larger TECs can be due to the increase of the ionic radius of Co during the thermal expansion measurement [40]. Similar results had been reported earlier for double-layered perovskite cathodes. For examples, the TECs in the temperature range of 30–1000 °C in air for $PrBaCo_2O_{5+\delta}$, $NdBaCo_2O_{5+\delta}$ and $SmBaCo_2O_{5+\delta}$ are 21.5×10^{-6} K^{-1}, 21.0×10^{-6} K^{-1} and 19.1×10^{-6} K^{-1}, respectively [41], the TEC of $GdBaCo_2O_5$ between 30 and 900 °C is 20.0×10^{-6} K^{-1} [42].

The temperature dependence of the electrical conductivity of SBSC-based samples in air is shown in Fig. 5. The conductivities decrease with increasing temperature exhibiting a metallic behavior for all samples. SBSC55 revealed a reduction of electrical conductivity from 300 °C due to lattice defects breaking the Co-O-Co bonds, resulting in escape of oxygen atoms from lattice and reduction of Co^{4+} to Co^{3+} or Co^{3+} to Co^{2+}, which corresponds to our previous TGA data. An abrupt reduction in electrical conductivity behavior also can be found SBSC73 above 420 °C. For SBSC91, the conductivity is reduced from 33.4 S/cm of 300 °C to 27.1 S/cm of 800 °C. The conductivity behavior for SBSC-based samples may be related to the following reasons [43–45]: (1) an energy band overlap between Co-3d and O-2p, (2) the presence of Co^{4+} ions from thermally generated charge disproportion of Co^{3+} and (3) the loss of oxygen from the lattice at higher temperatures.

In SBSC-based cathodes, the major defects are the oxygen interstitials, O_i'' and the electronic holes, $h = Co_{Co}$ [46]. Using the Kroger-Vink notation, the formation of the oxygen interstitials and

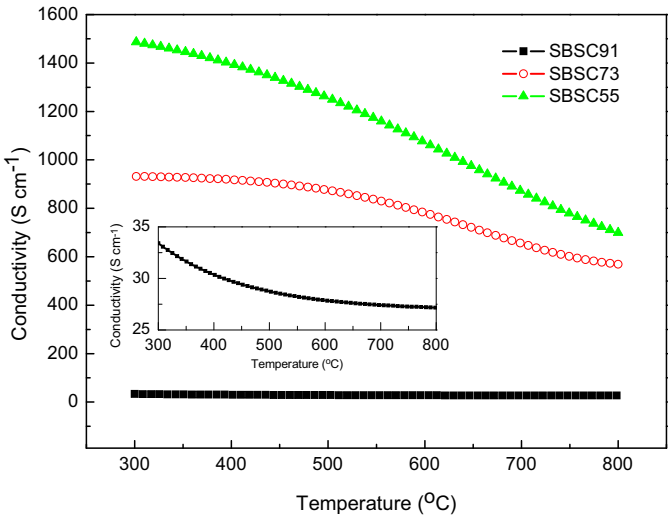

Fig. 5. Temperature dependence of the electrical conductivity in air for SBSC-based cathodes. The inset shows the detail of the electrical conductivity in air as a function of temperature for SBSC91.

electronic hole is expressed by

$$\frac{1}{2}O_2 + Co_{Co}^{\times} \leftrightarrow O_i'' + 2Co_{Co}^{\cdot} \quad (2)$$

The electrical neutrality condition is given by

$$2[O_i''] = [Co_{Co}^{\cdot}] \quad (3)$$

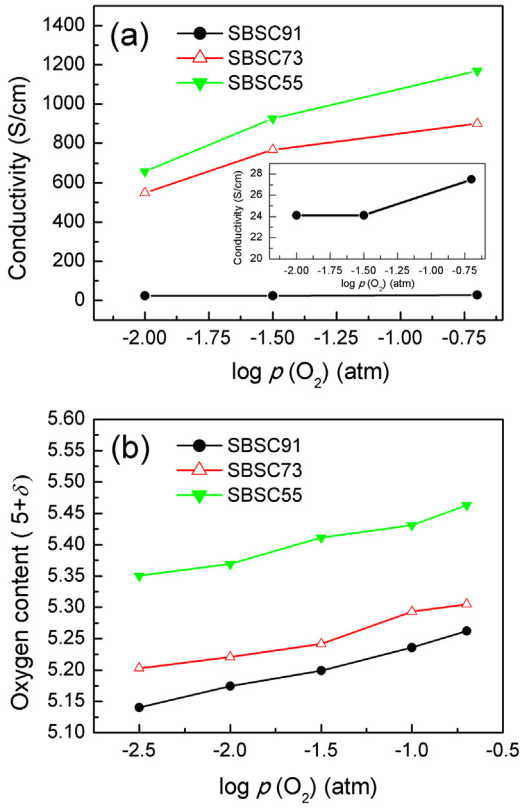

Fig. 6. (a) Electrical conductivity and (b) oxygen content (5 + δ) of SBSC-based cathodes at various $p(O_2)$ at 600 °C. The inset in (a) reveals the detail of the electrical conductivity as a function of $p(O_2)$ for SBSC91.

At a given temperature, the electrical conductivity values are in the order as follows: SBSC55 > SBSC73 > SBSC91. This behavior might be due to the increasing electronic hole associated with oxygen content. Based on defect Equations (2) and (3), the electrical conductivity is proportional to $p(O_2)$ with the power of 1/6. For SBSC73 and SBSC55, both specimens are valid for Equation (2). However, SBSC91 is invalid for the equation. It is presumed that the main compensation mechanism is due to creation of $V_O^{\cdot\cdot}$ and instead of $Co_{Co}^{\cdot}$ in equation (2). This behavior is consistent with oxygen content (5 + δ) result. Apparently, SBSC55 with highest oxygen content possessed a maximum conductivity, SBSC91 possessed lower 5 + δ and electrical conductivity due to creation of higher amount of oxygen vacancy.

Fig. 6 shows the temperature dependence of the electrical conductivity and oxygen content of the SBSC-based cathodes at various oxygen partial pressure ($p(O_2)$). With decreasing $p(O_2)$, the electrical conductivities decrease with $p(O_2)$. This may be ascribed to the decreasing concentration in mobile interstitial oxygen at lower $p(O_2)$ [47]. Understanding the electrical conductivity of cathodes at low $p(O_2)$ is very important to make sure efficient current collection and long-term stability [48]. The decrease in the interstitial oxygen concentration by lowering $p(O_2)$ leads a reduction in electronic holes; the decrease in electronic holes is significantly related to lower electronic conductivities at lower $p(O_2)$. The $p(O_2)$ dependence of the electrical conductivity of SBSC cathode at 600 °C simultaneously is plotted in Fig. 6(a). The electrical conductivities of SBSC55 at 600 °C are distributed in the range of 660 S/cm of $p(O_2) = 0.01$ atm to 1168 S/cm of $p(O_2) = 0.21$ atm, indicating that SBSC55 can endure low $p(O_2)$. Fig. 6(b) shows the oxygen content of SBSC-based cathodes determined by TGA as a function of $p(O_2)$ at 600 °C. The higher redox stability as well as electrical conductivity are very important for cathode materials under operating conditions of IT-SOFC. The decrease in oxygen content was due to a partial loss of lattice oxygen, so that the oxygen content is highly related to composition, temperature and oxygen pressure. The degree of oxygen-content reduction as function of $p(O_2)$ is in correspondence with structure redox

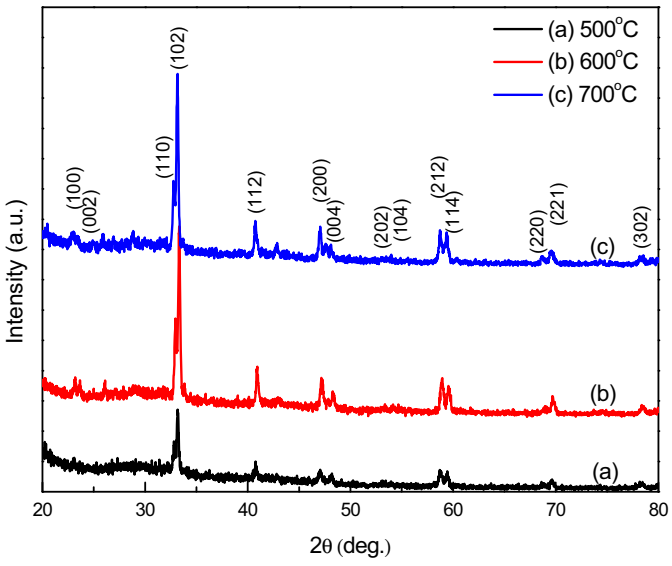

Fig. 7. X-ray diffraction patterns of SBSC55 sintered specimens after exposure to $p(O_2) = 0.01$ atm in the temperature range of 500–700 °C for 4 h.

stability. The reduced-rate in oxygen content $(5+\delta)$ from $p(O_2)=0.21$ to 3×10^{-3} atm at 600 °C, R, was defined as the following equation:

$$R = \frac{(5+\delta)_{p(O_2)=0.21} - (5+\delta)_{p(O_2)=3\times10^{-3}}}{(5+\delta)_{p(O_2)=0.21}} \quad (4)$$

Here $(5+\delta)_{p(O_2)=0.21}$ and $(5+\delta)_{p(O_2)=3\times10^{-3}}$ indicate the oxygen content at $p(O_2)=0.21$ atm and 3×10^{-3} atm, respectively a 600 °C. Among the SBSC-based cathodes, SBSC55 shows the lowest reduced-rate of 1.81% in oxygen content from $p(O_2)=0.21$ to 3×10^{-3} atm.; whereas, the reduced-rate in oxygen content for SBSC73 and SBSC91 is 2.05 and 2.06%, respectively. This implies that SBSC55 has better durability in reducing atmosphere under cathodic polarization, and the SBSC55 is suitable cathode for application in IT-SOFC. It is interesting that SBSC55 specimen exhibited high electrical conductivity in low oxygen partial pressure. Generally, the electrical conductivity in low oxygen partial pressure is highly related to the structure stability. Therefore, the phase stability of cathodes in low oxygen partial pressure is necessary to identify. In this study, SBSC55 sintered specimens were exposed to $p(O_2)=0.01$ atm in the temperature range of 500–700 °C for 4 h and characterized their phases by XRD as shown in Fig. 7 Obviously, the SBSC55 revealed majority of double perovskite structure with minority of secondary phase after specimens exposures to $p(O_2)=0.01$ atm. SBSC55 with high electrical conductivity in $p(O_2)=0.01$ atm is due to the fact that SBSC55 still retains double perovskite structure at such low oxygen partial pressure.

Fig. 8 presents some typical impedance spectra of SBSC|SDC|SBSC symmetrical cells using AC impedance spectroscopy under open circuit conditions at various temperatures in air. The R_p values decrease significantly with increasing temperature for all samples showing the ORR of SBSC cathode is a thermally activated process. The R_p values represent cathodic properties including oxygen reduction reaction at low temperatures, oxygen surface/bulk diffusion and the gas phase oxygen diffusion at high temperatures [49]. The R_p values of SBSC cathode decrease with increasing Sr content. The R_p values of SBC91, SBSC73 and SBSC55 are 2.04, 1.81 and 0.57 Ω cm^2, respectively at 750 °C. The R_p of SBSC55 cathode revealed the lowest values for all temperatures, indicating that high oxygen-ion transports in the interface between SBSC55 and SDC electrolyte. For SBSC55, the R_p values reduced from 4.17 Ω cm^2 of 600 °C to 0.35 Ω cm^2 of 800 °C.

Fig. 9 revealed the single cell performances for anode-supported Ni-SDC|SDC|SBSC SOFC using humidified hydrogen (3 vol% H_2O) as the fuel and air as the oxidant. In general, the cell voltage was reduced with the increasing temperature; however, current density and the maximum power densities were increased with the increasing temperature due to the thermally activated process of kinetics [50]. Generally, the open-circuit voltage (OCV) of an ideal cell should be close to its theoretic value of 1.1 V, and slightly influenced by the operating condition. In this study, the OCV values were lower than the theoretical value, which

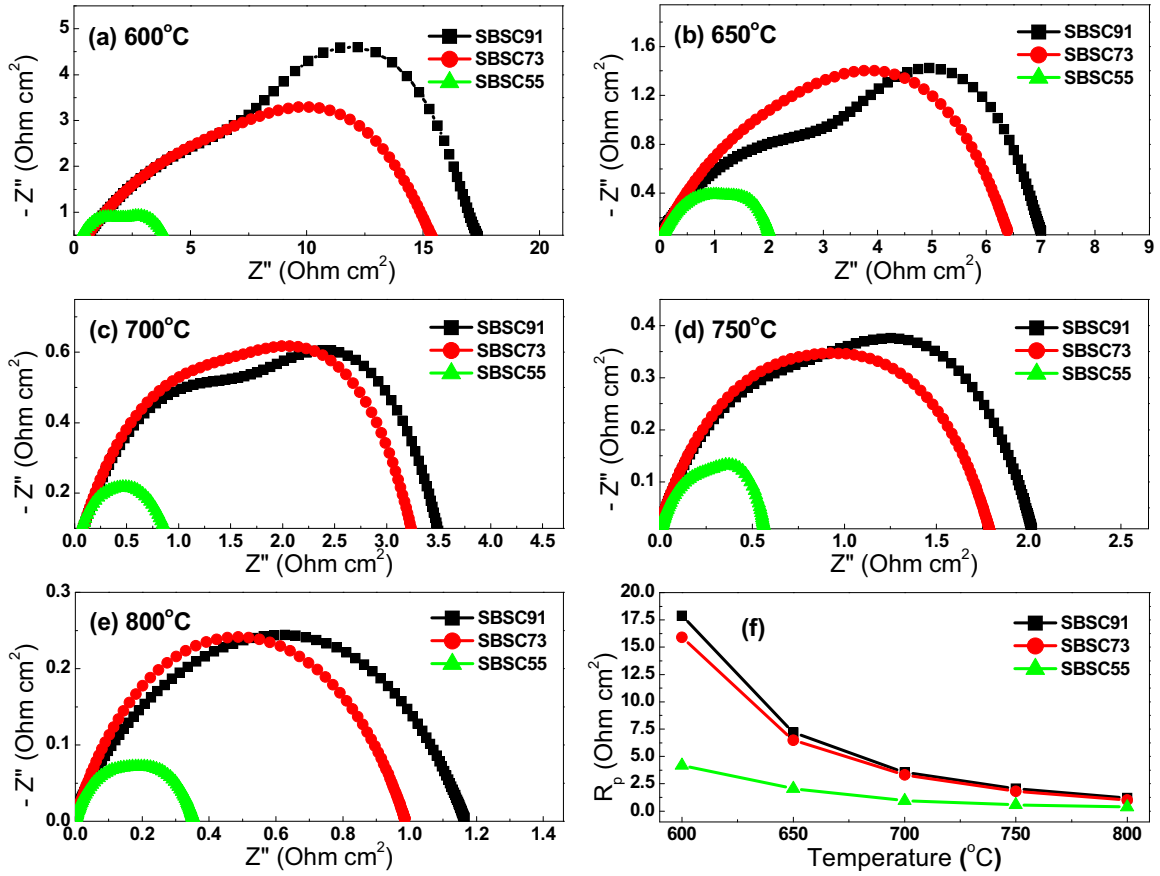

Fig. 8. Typical impedance spectra of SBSC-based cathodes on SDC electrolytes at (a) 600, (b) 650, (c) 700, (d) 750, (e) 800 °C and (f) total cathode polarization resistance (R_p) over the temperature range of 600–800 °C.

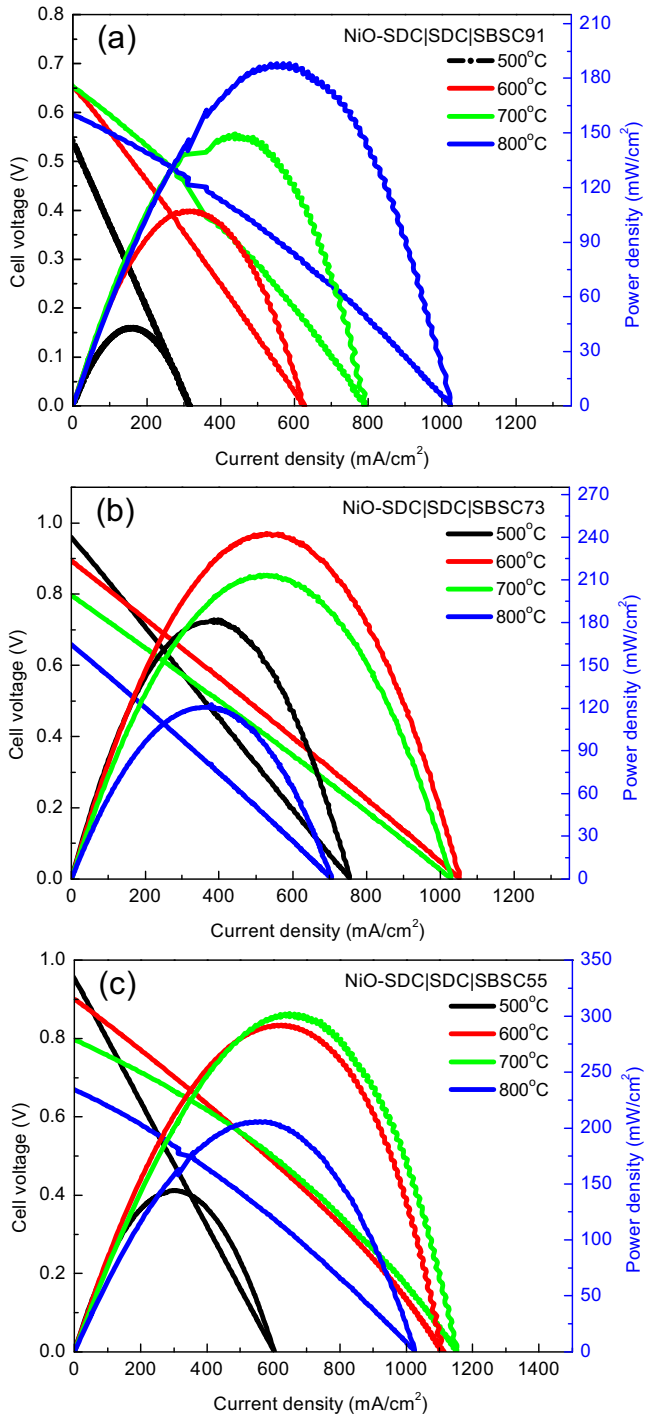

Fig. 9. I–V curve for single cells of (a) Ni-SDC|SDC|SBSC91, (b) Ni-SDC|SDC|SBSC73 and (c) Ni-SDC|SDC|SBSC55 under H_2 fuel and air oxidant in the temperature range of 500–800 °C.

might be ascribed to the following reasons. (1) Ce^{4+} in SDC electrolyte easily reduces to Ce^{3+} especially at higher temperature. Based on chemical defect concept, it can be described by the following equation:

$$Ce_{Ce} \rightarrow Ce'_{Ce} + h^{\cdot} \quad (5)$$

The SDC electrolyte with a low electronic conductivity leading a slight electron cross flow (current leakage) might occur through the electrolyte, and (2) fuel/oxidant may cross through the electrolyte membrane due to the some porosities and the current leakage resulting in a lower cell OCV.

Among the SBSC-based cathodes, SBSC55 shows the highest power densities from 500 to 800 °C. The peak powder densities at operating temperature of 700 °C reach 149, 242 and 304 mW/cm^2 for SBSC91, SBSC73 and SBSC55, respectively. For SBSC73 and SBSC55, the peak power densities revealed at operating temperature of 700 °C; whereas the peak power densities were reduced above 700 °C. This behavior is associated to lower OCV values occured at higher temperature (800 °C) as shown in Fig. 9(b) and (c). The single cell performance is improved with increasing the substitution amount of Sr for Ba in $SmBa_{1-x}Sr_xCo_2O_{5+\delta}$ cathodes. The peak power densities of SBSC55 are 144, 292, 304 and 206 mW cm^{-2} at 500, 600, 700 and 800 °C, respectively. The layered-perovskite $SmBa_{1-x}Sr_xCo_2O_{5+\delta}$ with higher Sr content ($x = 0.5$) in the A-site are thought to have rapid oxygen kinetics due to reduced oxygen bonding strength in the [AO] layer and a disorder-free channel for ion diffusion, and the phenomenon will improve cathode performance such as electrical conductivity, electrochemical properties as well as further performance in single cell [26].

The SEM images of cross-section view and surface view for SBSC55 cathode are shown in Fig. 10. The microstructure of a cross section of SBSC55|SDC|Ni–SDC showed a 20 μm of SBSC55 cathode and a 15 μm of SDC electrolyte as seen in Fig. 10(a). The adhesion between the cathode and electrolyte is quite good. The SBSC55 particles distributed uniformly and the particle size is in the range of 1–2 μm. The cathode microstructure is closely related to the characteristics of the surface area and electron transport. These properties influence the performance of fuel cell such as the reaction kinetics, charge transport, and mass transport preprocess [51,52]. The porosity as shown in Fig. 10(b), the SBSC55 cathode provides in plenty of TPB sites for electrochemical reaction.

4. Conclusions

This study mainly investigated the effect of Sr doping on $SmBaCo_2O_{5+\delta}$ with regard to structural characteristics, thermal expansion behavior, electrical conductivity and electrochemical properties. The TEC values of SBSC-based cathodes decrease with Sr content revealing the TEC values of 19.8–20.5 $\times 10^{-6}$ K^{-1} in the temperature range of 100–800 °C. SBSC55 with high electrical conductivity in $p(O_2) = 0.01$ atm is ascribed to SBSC55 with stable double-perovskite structure at such low oxygen partial pressure. The R_p of SBSC55 revealed the lowest values for all temperatures, indicating that high oxygen-ion transports in the interface between SBSC55 and SDC electrolyte. The single cell performance is improved with increasing the Sr content for SBSC-based cathodes. The maximum powder densities of anode-supported single cell with SBSC as cathode at operating temperature of 700 °C can reach 149, 242 and 304 mW/cm^2 for SBSC91, SBSC73 and SBSC55, respectively. Sr properly substituting for Ba in SBSC can reduced TEC values, and enhance electrical properties, redox stability and electrochemical performance. SBSC55 could be considered a potential cathode materials for IT-SOFC

Acknowledgements

The authors would like to thank Ministry of Science and Technology of Taiwan for financially supporting this research under contract number: MOST 103-2113-M-259-002, MOST 104-2119-M-259-003 and MOST 104-2113-M-259-005.

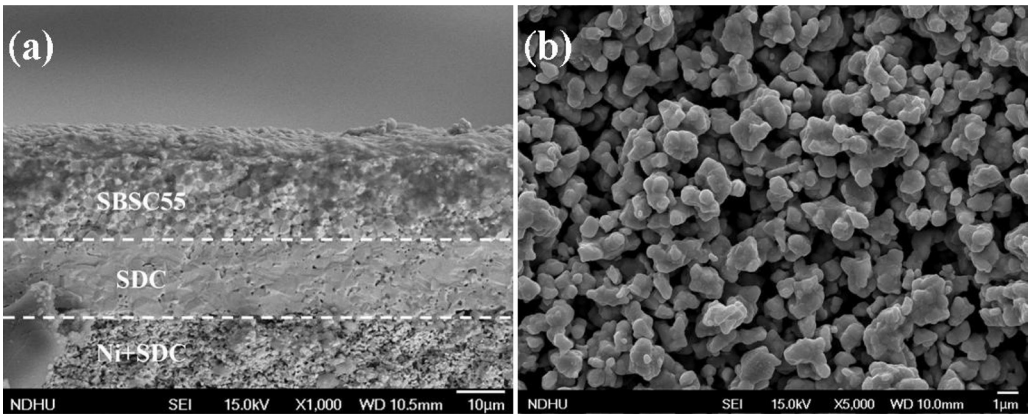

Fig. 10. SEM image SBSC55 cathode in the single cell: (a) cross-section view and (b) surface view.

References

[1] D. Ding, X. Li, S.Y. Lai, K. Gerdes, M. Liu, Enhancing SOFC cathode performance by surface modification through infiltration, Energy Environ. Sci. 7 (2014) 552–575.

[2] B.C.H. Steele, A. Heinzel, Materials for fuel-cell technologies, Nature 414 (2001) 345–352.

[3] Y.H. Huang, R.I. Dass, Z.L. Xing, J.B. Goodenough, Double perovskites as anode materials for solid-oxide fuel cells, Science 312 (2006) 254–257.

[4] H. Moon, S.D. Kim, S.H. Hyun, H.S. Kim, Development of IT-SOFC unit cells with anode- supported thin electrolytes via tape casting and co-firing, Int. J. Hydrogen Energy 33 (2008) 1758–1768.

[5] M.T. Colomer, B.C.H. Steele, J.A. Kilner, Structural and electrochemical properties of the $Sr_{0.8}Ce_{0.1}Fe_{0.7}Co_{0.3}O_{3-\delta}$ perovskite as cathode material for ITSOFCs, Solid State Ionics 147 (2002) 41–48.

[6] A. Jun, J. Shin, G. Kim, High redox and performance stability of layered $SmBa_{0.5}Sr_{r0.5}Co_{1.5}Cu_{0.5}O_{5+\delta}$ perovskite cathodes for intermediate-temperature solid oxide fuel cells, Phys. Chem. Chem. Phys. 15 (2013) 19906–19912.

[7] L. Jiang, T. Wei, R. Zeng, W.X. Zhang, Y.H. Huang, Thermal and electrochemical properties of $PrBa_{0.5}Sr_{0.5}Co_{2-x}Fe_xO_{5+\delta}$ (x = 0.5 1.0, 1.5) cathode materials for solid-oxide fuel cells, J. Power Sources 232 (2013) 279–285.

[8] N.P. Brandon, S. Skinner, B.C.H. Steele, Recent advances in materials for fuel cells, Ann. Rev. Mater. Res. 33 (2003) 183–213.

[9] Q. Zhou, T. He, Y. Ji, $SmBaCo_2O_{5+x}$ double-perovskite structure cathode material for intermediate-temperature solid-oxide fuel cells, J. Power Sources 185 (2008) 754–758.

[10] Y. Takeda, R. Kanno, M. Noda, Y. Tomida, O. Yamamoto, Cathodic polarization phenomena of perovskite oxide electrodes with stabilized zirconia, J. Electrochem. Soc. 134 (1987) 2656–2661.

[11] S.B. Adler, Factors governing oxygen reduction in solid oxide fuel cell cathodes, Chem. Rev. 104 (2004) 4791–4843.

[12] S.B. Adler, J.A. Lane, B.C.H. Steele, Electrode kinetics of porous mixed-conducting oxygen electrodes, J. Electrochem. Soc. 143 (1996) 3554–3564.

[13] J.H. Kim, J.T.S. Irvine, Characterization of layered perovskite oxides $NdBa_{1-x}Sr_xCo_2O_{5+}$ (x = 0 and 0.5) as cathode materials for IT-SOFC, Int. J. Hydrogen Energy 37 (2012) 5920–5929.

[14] C. Kuroda, K. Zheng, K. Swierczek, Characterization of novel $GdBa_{0.5}Sr_{0.5}Co_{2-x}Fe_xO_{5+\delta}$ perovskites for application in IT-SOFC cells, Int. J. Hydrogen Energy 38 (2013) 1027–1038.

[15] L. Jiang, T. Wei, R. Zeng, W.X. Zhang, Y.H. Huang, Thermal and electrochemical properties of $PrBa_{0.5}Sr_{0.5}Co_{2-x}Fe_xO_{5+\delta}$ (x = 0.5 1.0, 1.5) cathode materials for solid-oxide fuel cells, J. Power Sources 232 (2013) 279–285.

[16] J. Xue, Y. Shen, T. He, Performance of double-proveskite $YBa_{0.5}Sr_{0.5}Co_2O_{5+\delta}$ as cathode material for intermediate-temperature solid oxide fuel cells, Int. J. Hydrogen Energy 36 (2011) 6894–6898.

[17] A.A. Taskin, A.N. Lavrov, Y. Ando, Achieving fast oxygen diffusion in perovskites by cation ordering, Appl. Phys. Lett. 86 (2005) 091910.

[18] A. Maignan, C. Martin, D. Pelloquin, N. Nguyen, B. Raveau, Structural and magnetic studies of ordered oxygen-deficient perovskites $LnBaCo_2O_{5+\delta}$, closely related to the '112' Structure, J. Solid State Chem. 142 (1999) 247–260.

[19] J.H. Kim, F. Prado, A. Manthiram, Characterization of $GdBa_{1-x}Sr_xCo_2O_{5+\delta}(0 \le x \le 1.0)$ double perovskites as cathodes for solid oxide fuel cells, J. Electrochem. Soc. 155 (2008) B1023–B1028.

[20] A. McKinlay, P. Connor, J.T.S. Irvine, W.Z. Zhou, Structural chemistry and conductivity of solid solution $YBa_{1-x}Sr_xCo_2O_{5+\delta}$, J. Phys. Chem. C. 111 (2007) 19120–19125.

[21] F. Meng, T. Xia, J. Wang, Z. Shi, J. Lian, H. Zhao, J.M. Bassat, J.C. Grenier, Evaluation of layered perovskites $YBa_{1-x}Sr_xCo_2O_{5+\delta}$ as cathodes for intermediate-temperature solid oxide fuel cells, Int. J. Hydrogen Energy 39 (2014) 4531–4543.

[22] Y.P. Fu, S.B. Wen, C.H. Lu, Preparation and characterization of samaria-doped ceria electrolyte materials for solid oxide fuel cells, J. Am. Ceram. Soc. 91 (2008) 127–131.

[23] A. Subardi, M.H. Cheng, Y.P. Fu, Chemical bulk diffusion and electrochemical properties of $SmBa_{0.6}Sr_{0.4}Co_2O_{5+\delta}$ cathode for intermediate solid oxide fuel cells, Int. J. Hydrogen Energy 39 (2014) 20783–20790.

[24] M. Kuhn, J.J. Kim, S.R. Bishop, H.L. Tuller, Oxygen nonstoichiometry and defect chemistry of perovskite-structured $BaxSr_{1-x}Ti_{1-y}Fe_yO_{3-y/2+\delta}$ Chem, Mater. 25 (2013) 2970–2975.

[25] Y.P. Fu, J. Ouyang, C.H. Li, S.H. Hu, Chemical bulk diffusion coefficient of $Sm_{0.5}Sr_{0.5}CoO_{3-\delta}$ cathode for solid oxide fuel cells, J. Power Sources 240 (2013) 168–177.

[26] A. Jun, J. Kim, J. Shin, G. Kim, Optimization of Sr content in layered $SmBa_{1-x}Sr_xCo_2O_{5+\delta}$ perovskite cathodes for intermediate-temperature solid oxide fuel cells, Int. J. Hydrogen Energy 37 (2012) 18381–18388.

[27] H. Falcon, J. Barbero, Double perovskite oxides A_2FeMoO_6 (A = Ca, Sr and Ba) as catalysts for methane combustion, Applied Catalysis B: Environmental 53 (2004) 37–45.

[28] M.M. Natile, F. Poletto, A. Galenda, A. Glisenti, T. Montini, L.D. Rogatis, P. Fornasiero, $La_{0.6}Sr_{0.4}Co_{1-y}Fe_yO_{3-\delta}$ perovskite: influence of the Co/Fe atomic ratio on properties and catalytic activity toward alcohol steam-reforming, Chem. Mater. 20 (2008) 2314–2327.

[29] L. Jiang, F. Li, T. Wei, R. Zeng, Y. Huang, Evaluation of $Pr_{1+x}Ba_{1-x}Co_2O_{5+\delta}$ ($x = 0 - 0.30$) as cathode materials for solid-oxide fuel cells, Electrochim. Acta 133 (2014) 364–372.

[30] P.A.W. Van der Heide, Systematic X-ray photoelectron spectroscopic study of $La_{1-x}Sr_x$-based perovskite-type oxides, Surf. Interface Anal. 33 (2002) 414–425.

[31] Q. Xu, D.P. Huang, W. Chen, H. Wang, B.T. Wang, R.Z. Yuan, X-ray photoelectron spectroscopy investigation on chemical states of oxygen on surfaces of mixed electronic-ionic conducting $La_{0.6}Sr_{0.4}Co_{1-y}Fe_yO_3$ ceramics, Appl. Surf. Sci. 228 (2004) 110–114.

[32] P. Meuffels, Propane gas sensing with high-density $SrTi_{0.6}Fe_{0.4}O_{3-\delta}$ ceramics evaluated by thermogravimetric analysis, J. Eur. Ceram. Soc. 27 (2007) 285–290.

[33] S. Lia, W. Jin, N. Xu, J. Shi, Mechanical strength, and oxygen and electronic transport properties of $SrCo_{0.4}Fe_{0.6}O_{3-d}$-YSZ membranes, J. Member. Sci. 186 (2001) 195–204.

[34] B. Wei, Z. Lu, S. Li, Y. Liu, K. Liu, W. Su, Thermal and electrical properties of new cathode material $Ba_{0.5}Sr_{0.5}Co_{0.8}Fe_{0.2}O_{3-\delta}$ for solid oxide fuel cells, Electrochem. Solid State Lett. 8 (2005) A428–A431.

[35] G.C. Kostogloudis, N. Vasilakos, C. Ftikos, Crystal structure, thermal and electrical properties of $Pr_{1-x}Sr_xCoO_{3-\delta}$ (x = 0, 0. 15, 0. 3, 0. 4, 0. 5) perovskite oxides, Solid State Ionics 106 (1998) 207–218.

[36] G. Kim, S. Wang, A.J. Jacobson, L. Reimus, P. Brodersen, C.A. Mims, Rapid oxygen ion diffusion and surface exchange kinetics in $PrBaCo_2O_{5+x}$ with a perovskite related structure and ordered A cations, J. Mater. Chem. 17 (2007) 2500–2505.

[37] K. Huang, H.Y. Lee, J.B. Goodenough, Sr- and Ni-Doped $LaCoO_3$ and $LaFeO_3$ perovskites: new cathode materials for solid oxide fuel Cells, J. Electrochem. Soc. 145 (1998) 3220–3227.

[38] M.A. Senaris-Rodriguez, J.B. Goodenough, $LaCoO_3$ revisited, J.Solid State Chem. 116 (1995) 224–231.

[39] J.H. Kim, F. Prado, A. Manthiram, Characterization of $GdBa_{1-x}Sr_xCo_2O_{5+\delta}$ double perovskites as cathodes for solid oxide fuel cells, J. Electrochem. Soc. 155 (2008) B1023–B1028.

[40] M. Mori, N.M. Sammes, Sintering and thermal expansion characterization of Al-doped and Co-doped lanthanum strontium chromites synthesized by the Pechini method, Solid State Ionics 146 (2002) 301–312.

[41] X. Che, Y. Shen, H. Li, T. He, Assessment of $LnBaCo_{1.6}Ni_{0.4}O_{5+\delta}$ (Ln = Pr Nd, and Sm) double-perovskites as cathodes for intermediate-temperature solid-oxide fuel cells, J. Power Sources 222 (2013) 288–293.

[42] B. Wei, Z. Lü, D. Jia, X. Huang, Y. Zhang, W. Su, Thermal expansion and electrochemical properties of Ni-doped $GdBaCo_2O_{5+\delta}$ double-perovskite type oxides, Int. J. Hydrogen Energy 35 (2010) 3775–3782.
[43] S. Park, S. Choi, J. Shin, G. Kim, Tradeoff optimization of electrochemical performance thermal expansion for Co-based cathode material for intermediate-temperature solid oxide fuel cells, Electrochim. Acta 125 (2014) 683–690.
[44] X. Zhang, H. Hao, X. Hu, Electronic transport properties of $YBaCo_{2-x}Cu_xO_{5+\delta}$ ($0 \leq x \leq 1$) at high temperature, Physica. B, Condensed matter 403 (2008) 3406–3409.
[45] S. Yoo, J.Y. Shin, G. Kim, Thermodynamic and electrical characteristics of $NdBaCo_2O_{5+\delta}$ at various oxidation and reduction states, J. Mater. Chem. 21 (2011) 439–443.
[46] S. Yoo, S. Choi, J. Kim, J. Shin, G. Kim, Investigation of layered perovskite type $NdBa_{1-x}Sr_xCo_2O_{5+\delta}$ (x = 0 0.25, 0.5, 0.75, and 1.0) cathodes for intermediate-temperature solid oxide fuel cells, Electrochim. Acta 100 (2013) 44–50.
[47] F. Mauvy, J.M. Bassat, E. Boehm, J.P. Manaud, P. Dordor, J.C. Grenier, Oxygen electrode reaction on $Nd_2NiO_{4+\delta}$ cathode materials: impedance spectroscopy study, Solid State Ionics 158 (2003) 17–28.
[48] D.M. Bastidas, S. Tao, J.T.S. Irvine, A symmetrical solid oxide fuel cell demonstrating redox stable perovskite electrodes, J. Mater. Chem. 16 (2006) 1603–1605.
[49] S.W. Baek, J.H. Kim, J. Bae, Characteristics of ABO_3 and A_2BO_4 (A = Sm, Sr; B = Co Fe, Ni) samarium oxide system as cathode materials for intermediate temperature-operating solid oxide fuel cell, Solid State Ionics 179 (2008) 1570–1574.
[50] M.B. Choi, K.T. Lee, H.S. Yoon, S.Y. Jeon, E.D. Wachsman, S.J. Song, Electrochemical properties of ceria-based intermediate temperature solid oxide fuel cells using microwave heated $La_{0.1}Sr_{0.9}Co_{0.8}Fe_{0.2}O_{3-\delta}$ as a cathode, J. Power Sources 220 (2012) 377–382.
[51] J.H. Nam, D.H. Jeon, A comprehensive microscale model for transport and reaction in intermediate temperature solid oxide fuel cell, Electrochim. Acta 51 (2006) 3446–3460.
[52] M. Andersson, J. Yuan, B. Sunden, Review on modeling development for multiscale chemical reactions coupled transport phenomena in solid oxide fuel cells, Appl. Energy 87 (2010) 1461–1476.